Journal Pre-proof

Graphene morphology effect on the gas barrier, mechanical and thermal properties of thermoplastic polyurethane

Muhammad Zahid, Antonio Esaú Del Río Castillo, Sanjay Balkrishna Thorat, Jaya Kumar Panda, Francesco Bonaccorso, Athanassia Athanassiou

PII: S0266-3538(20)32251-X

DOI: https://doi.org/10.1016/j.compscitech.2020.108461

Reference: CSTE 108461

To appear in: *Composites Science and Technology*

Received Date: 19 May 2020

Revised Date: 31 August 2020

Accepted Date: 13 September 2020

Please cite this article as: Zahid M, Del Río Castillo AE, Thorat SB, Panda JK, Bonaccorso F, Athanassiou A, Graphene morphology effect on the gas barrier, mechanical and thermal properties of thermoplastic polyurethane, *Composites Science and Technology*, https://doi.org/10.1016/j.compscitech.2020.108461.

31/08/2020

Dear Editor,

We have carefully revised our manuscript, considering the Reviewers' comments. We stress that the results are the same as in the previous version submitted but enriched with the specific information required by the reviewers.

Best Regards

The Authors

Graphene morphology effect on the gas barrier, mechanical and thermal properties of thermoplastic polyurethane

Muhammad Zahid[1], Antonio Esaú Del Río Castillo[2], Sanjay Balkrishna Thorat[2], Jaya Kumar Panda[2], Francesco Bonaccorso[2,*], Athanassia Athanassiou[1,*]

[1] Smart Materials, Istituto Italiano di Tecnologia, Via Morego 30, Genoa 16163 Italy

[2] Graphene Labs, Istituto Italiano di Tecnologia, Via Morego 30, Genoa 16163 Italy

Abstract: In this study, we investigated the effect of the morphology of few-layer (FLG) and multi-layer (MLG) graphene flakes on the gas barrier properties of thermoplastic polyurethane (TPU) films. Composite films of TPU filled with FLG and MLG at different concentrations are prepared by solution blending-casting and hot-pressing, achieving an in-plane alignment of the fillers and, consequently, improving the gas barrier properties. Specifically, the hot-pressed TPU composites loaded with 4 wt.% of the MLG with a lateral size distribution of 0.1-25.0 μm demonstrates a reduction of ~81% in the gas permeability compared to the pristine TPU. Additionally, the thermal conductivity of the TPU composite (loaded with 4 wt.% of MLG) is enhanced ~3 times and the Young modulus increases more than 5 times compared to the pristine TPU.

Keywords: Composites, gas barrier, graphene, polyurethane, thermal conductivity

***Corresponding authors:** Athanassia.Athanassiou@iit.it (Athanassia Athanassiou)

Francesco.Bonaccorso@iit.it **(**Francesco Bonaccorso)

1. Introduction

Petrochemical-based plastics are widely used worldwide in many applications, *e.g.*, constructions[1], aerospace[2], automotive[3], energy devices[4], and packaging[5,6]. Thanks to their excellent characteristics, *i.e.*, high strength to weight ratio (*e.g.*, specific strength of aramid fiber is 3.0 GPa (g cm^{-3}) as compared to 0.3 GPa (g cm^{-3}) for steel))[7], ease of processing and resistant to corrosion, as well as their low cost. Plastics have partially or entirely replaced metals or alloys in several applications[8,9]. In particular, more than one-third of the plastics global production is used in packaging for food and electronics, being this the primary field for plastic use[10]. However, most of the plastic materials do not degrade in nature over time[8,11]. The lack of degradability, combined with recycling issues and shrinking landfill sites, has raised severe environmental problems worldwide[8]. Therefore, alternative products with zero or reduced ecological impact and performances comparable to the currently used polymers have consistently been sought[12].

Recently, polyurethanes (PUs) have garnered the attention of the researchers and industries since they are considered highly versatile polymers, being biocompatible and biodegradable[13–15]. Thermoplastic PUs (TPUs) also demonstrate high stretchability (> 600%), high tear resistance (~130 N mm^{-1})[16], excellent chemical resistance to oils, greases and solvents[13], ease in processability, and good weather stability, as is typical of elastomers[17,18]. Nevertheless, virgin TPUs are highly permeable to gas molecules and, therefore, are unsuitable for packaging and storage applications[19,20]. The oxygen permeability in packaging materials must be as low as possible to enhance the shelf life of the package content[5]. In the past, different zero-dimensional (0D), *e.g.,* silica nanoparticles[21,22], one-dimensional (1D), *e.g.*, carbon nanotubes[23], two-dimensional (2D) crystals, *e.g.*, graphene[24], layered-silicates[18,25], hexagonal boron nitride flakes[26], defective 2D crystals (graphene oxides (GO) and reduced graphene oxides (RGO)[27–31]), and three dimensional (3D) fillers, *e.g.*, segregated graphene nanoplatelets (stacked up graphene layers or simply graphite) [32,33] have been successfully incorporated into polymer films

to enhance their gas barrier properties. In particular, the 2-D structures, having platelet geometry and high aspect ratio (α: the ratio of lateral size -L- to thickness -W- of the filler[24]), create a maze-like (or tortuous) path for gas molecules, delaying or eventually impeding the pass through the polymer films, resulting in superior gas barrier properties[20,34,35]. For example, PU composites enriched with organoclays (hexadecyl amine-montmorillonite, C_{16}-MMT) have achieved a 50% reduction of O_2 gas permeability with 4 wt.% fillers' content[36]. Similarly, the addition of defective 2-D crystals, *i.e.*, RGO into TPU, achieved a ~89% reduction in oxygen permeability at 2 wt.% mass loading. For this application, RGO (with average lateral size ~10 μm and an aspect ratio α ~ 30,000) was combined with TPU using a melt mixing method[29]. The as-prepared TPU/RGO composites also demonstrated a ~200 % increase in Young's modulus (from 5.5 MPa for pristine PU to 16.6 MPa), but with a reduction of the elongation at break from 385% to 218%[29]. Other studies demonstrated >90% reduction in the gas permeability of the TPU composites using carbon-based 2D fillers (*i.e.*, graphene, RGO, or GO) having aspect ratios ≥ 300[28,37]. These high-aspect-ratio fillers are costly (*e.g.*, ~10^5 $/gram for single-layer or bi-layer graphene)[38], thus not being cost-effective for gas barrier applications. In contrast, the commercially available crystalline graphene-based materials are often multi-layer (MLG) or graphene nanoplatelets (>8 carbon layers)[38,39] with broad size distributions, ranging from hundreds of nanometers to few tens of micrometers in lateral size[38,39]. These MLG flakes have affordable cost (0.5 – 2.0 $/gram),[38,40] being used in polymer composites to enhance their gas barrier[34,35], mechanical[41,42], electrical[43], and thermal properties[44,45]. However, a full understanding of the role of the filler morphology (*i.e.*, lateral size distribution -D_L- and thickness) in the final composite properties (*i.e.*, gas barrier, mechanical and thermal) is still missing.

In this study, we investigated the dependence of the gas barrier properties of thermoplastic polyurethane (TPU) films on the concentration, in-plane alignment, and morphology of few-layer graphene (FLG) and MLG fillers. In particular, the hot-pressed TPU composites loaded with 4 wt.% of the MLG demonstrated a reduction of ~81% in the gas permeability compared to the pristine

TPU. Additionally, the thermal conductivity of the TPU composite (loaded with 4 wt.% of MLG) is enhanced ~3 times, and the Young modulus increases more than 5 times compared to the pristine polymer.

2. Materials and methods

2.1 Materials

Polyether-based aliphatic TPU (ELASTOLAN L1185 A12) was purchased from BASF, Germany, and used without further modifications. Two different types of MLG powders (> 8 carbon layers) were obtained from Strem Chemicals and Avanzare. Few-layer graphene (3-5 carbon layers) and another MLG powder were produced via the Wet Jet Milling process, as described in[46,47]. Chloroform ($CHCl_3$) 99.9% analytical grade was purchased from Merck and used as received.

2.2 Characterization of graphene materials

The FLG and MLG powders were characterized morphologically. The results are summarized in **Table 1**. The details on the characterization procedures are given in **Supporting Information, SI-1** (see also **Figure S1**).

Table 1. Morphological properties of the graphene powders.

Material	Lateral size L (nm)	Log-normal s.d.	Lateral size range D_L (μm)	Thickness W (nm)	Log-normal s.d.	Aspect ratio α=L/W	Bulk density δ (g cm^{-3})
FLG1	460	0.90	0.1-8.5	1.6	1.04	287	0.05
MLG1	415	1.05	0.1-9.5	5.3	0.80	78	0.06
MLG2	740	0.90	0.1-14.5	12.0	0.70	61	0.05
MLG3	300	1.20	0.1-25.0	5.6	0.84	53	0.01

The lateral size distribution (D_L) of the graphene-based flakes used as composite fillers is a key parameter to consider, especially for gas barrier applications. A large D_L range indicates the presence of fillers of significantly different sizes (*e.g.*, MLG3 contains flakes from 0.1 to 25.0 μm). In the polymer composites, aspect ratio, orientation, and size distribution of the fillers play

paramount roles in the packing density of the fillers (*i.e.*, number of fillers per unit area)[48]. An *in-plane* orientation of the fillers (see **Figure 1a**) exhibit improved packing density as compared to the randomly distributed fillers (see **Figure 1b**) and thus, superior gas barrier properties[49]. In the graphene-based polymer composites, it is challenging to control the orientation of the fillers, and in reality, they are randomly arranged throughout the polymer matrix[50]. Consequently, in a randomly arranged system, graphene-based with uniform lateral size and high aspect ratio cannot fill up the interspaces between the adjacent flakes, as illustrated in **Figure 1b**. However, in the case of graphene with a broad lateral size distribution such as MLG3, in which small-sized flakes are also present, can easily approach the interspaces and make highly tortuous paths for the diffused gas molecules (see **Figure 1c**).

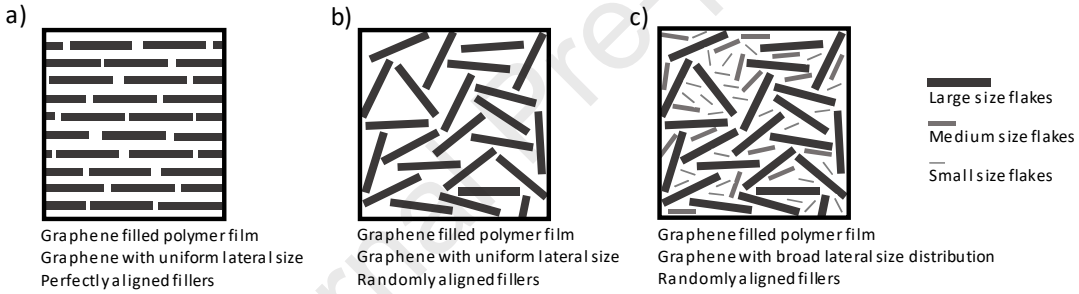

Figure 1. Schematic illustration of the orientation of the fillers inside a polymer matrix having different morphologies (lateral size).

2.3 Preparation of TPU/graphene-based composites

The TPU pellets were dissolved in 100 mL of $CHCl_3$ at 10 wt.% concentration. The TPU- $CHCl_3$ mixture was agitated overnight at room temperature using a magnetic stirrer. Then, the graphene-based powders were dispersed in $CHCl_3$ at 1 wt.% concentration using an ultrasonic bath operating at 59 Hz frequency and 100% amplitude for 3 h (SAVATEC, Strumenti Scientific). Subsequently, the TPU/graphene-based mixtures were prepared through solution blending as follows, 1, 2, 3, 4, and 5 mL of FLG1, MLG1, MLG2, and MLG3 graphene dispersion were mixed with 10 mL TPU solution constituting 1, 2, 3, 4, and 5 wt.% concentrated dispersion, respectively. The as-prepared TPU/graphene-based dispersions were further sonicated for 2 h and then probe-sonicated (Sonic,

Vibra cells, USA) for 30 s operating at 20 kHz frequency and 40% amplitude, before being transferred into the polytetrafluoroethylene Petri dishes. A schematic illustration of the fabrication process of the TPU/graphene-based composites is shown in **Figure 2**. The casted dispersions were left under aspiration hood overnight. After complete evaporation of the solvent, the as-prepared TPU/graphene-based composites were placed into the vacuum oven to remove residual solvents (at 65 °C and 1 bar vacuum pressure for 30 min). Afterward, the as-prepared TPU/graphene-based samples were conditioned at 23 °C and relative humidity (RH) ~65% for 24 h before the characterization processes. Selected samples were also hot pressed (Carver Press, TecnoVetro Srl Italy) at 130 °C under 3.0 metric tons for 30 min. Hereafter, TPU/graphene-based composites will refer to both TPU/FLG and TPU/MLG composites, unless stated otherwise.

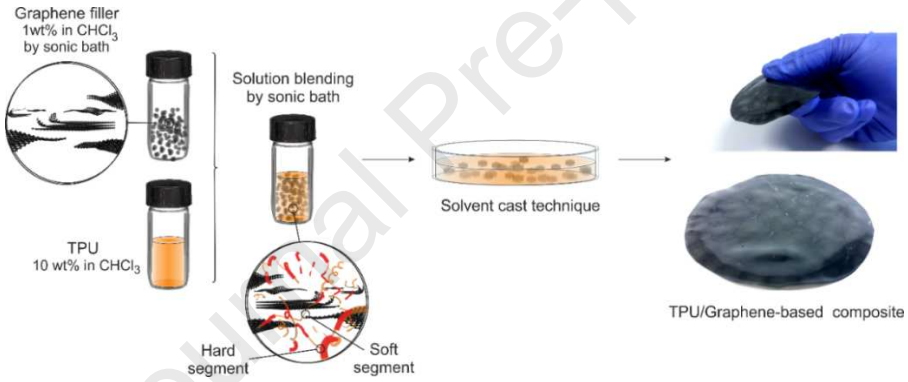

Figure 2. A schematic fabrication process of TPU/graphene-based composites.

2.4 Characterization of the composites

The cross-sectional morphology of the as-prepared composites was characterized by an analytical (low vacuum) scanning electron microscope using a JSM-6490LA SEM (JEOL) operating at 10 kV acceleration voltage. The TPU/graphene-based composites were also prepared for the SEM analysis with and without TPU skin to analyze the surface and bulk morphologies, respectively. Approximately 15 μm TPU skin was removed (see **supporting information, Figure S2**) using Leica UC6 ultramicrotome. The acquired SEM images were further analyzed using the image processing and analysis software ImageJ. Raman measurements were carried out using a Renishaw InVia micro-Raman spectrometer with a 50× objective (numerical aperture of 0.75), an excitation

wavelength of 514 nm line of an Ar^+ laser, and an incident power less than 1 mW. Mechanical properties of the composites were studied with an Instron dual column tabletop universal testing system 3365 (USA) at 50 mm/min strain rate according to ASTM D3505 standard test methods. The gas permeability of the as-prepared composites was measured with an Oxysense 5250i device (Oxysense) according to ASTM method F3136-15 (ASTM 1989). The test was performed at room conditions (23 °C, 50% RH). Ten readings were taken for each sample with a minimum coefficient of determination (R^2) value of ≥ 0.995. The O_2 gas permeability values have been reported in mL·micron/m^2·day·atm at STP (1 Barrer = 1 × 10^{10} cm^3·cm/cm^2·sec·cmHg or 6.58 × 10^4 mL·micron/m^2·day·atm at STP)[51,52]. Thermogravimetric analysis (TGA) was performed with a TGA Q500 (TA Instruments).

Through-plane thermal conductivity of the TPU/graphene-based composites was measured using a modified transient-plane source technique on a thermal conductivity analyzer (C-Therm Technologies, TCi) following ASTM D7984[53,54].

3. Results and discussion

3.1 Scanning electron microscopy (SEM)

The SEM images of the neat TPU and TPU/graphene-based composites loaded with FLG1, MLG1, MLG2, and MLG3 are shown in **Figure 3**. For brevity, the TPU/graphene-based composites at 4 wt.% of the filler content are presented herein for comparison purposes. The cross-sectional SEM images of the neat TPU and TPU/graphene-based composites appear to be significantly different from each other, as shown in **Figure 3a-e**. The cross-sectional SEM image of the neat TPU demonstrates a homogeneous layer of the polymer. On the contrary, the TPU/graphene-based composites display different surface topologies depending on the incorporated fillers. The sample TPU/FLG1 loaded with 4 wt.% of the FLG shows uniformly dispersed nanofillers, as shown in **Figure 3b**. Since the FLG1 sample has a small lateral size distribution D_L ≈ 0.1-8.5 μm and thickness 1.6 nm (as compared to MLG3 fillers D_L ≈ 0.1-25.0 μm, see **Table 1**), the graphene sheets create a less tortuous network compared to the MLG3 composites (see SEM images, **Figure 3e**).

Also, the TPU composites filled with MLG1 and MLG2 powders display aggregated platelets throughout the TPU matrices with several graphene-free TPU regions, as visible in **Figure 3c** and **3d**. The graphene-free regions lack maze-like paths for gas diffusion and are expected to present minimal resistance to the diffused gas molecules resulting in low gas barrier properties, as it will be demonstrated lines below. In **Figure 3e,** the TPU nanocomposite prepared with MLG3, which has a broad lateral size distribution ($D_L \approx$ 0.1-25.0 μm and thickness 5.6 nm), shows a higher filler packing (as compared to the other multilayer fillers, *i.e.*, MLG1 and MLG2) throughout the TPU polymer matrix with 4 wt.% of the fillers. In fact, the MLG3 flakes appear all over the cross-section of the composites. An image treatment software was used to determine the fraction area of the graphene-based flakes compared to the polymer matrix[55]. The analysis shows that the cross-section area of the TPU/MLG3 sample (**Figure 3e**) is composed of 17% of MLG3 fillers. Whereas, samples TPU/FLG1, TPU/MLG1, and TPU/MLG2 are composed of 11%, 12%, and 7% of graphene-based fillers, respectively (seen **Figure 3b-d)**. The as-prepared TPU composites (at 4 wt.%) did not show dispersion gradient through the film thickness except the TPU/MLG2 composite that displayed minor segregation of the fillers towards the bottom part (see **supporting information, Figure S3**). It is also important to note here that the cross-section of the sample TPU/MLG3 shows a higher number of graphene-based flakes per unit area (or packing density) compared to the other two multilayer fillers (MLG1 and MLG2), creating gas barriers inside the polymer matrix. This can be associated with the low bulk density of the MLG3 powder (0.012 $g \cdot cm^{-3}$), which is 4 to 5 times lighter than the other fillers (see **Table 1**). Therefore, the combination of low bulk density and broad lateral size distribution of the MLG3 powder results in more populated regions inside the composite, which create highly tortuous paths as compared to the FLG1, MLG1, and MLG2 fillers.

SEM analysis of the corresponding top surfaces also shows the surface appearance of the TPU and TPU/graphene-based composites. For example, the as-prepared neat TPU shows neither beads nor pores, see **Figure 3f**. However, on filler inclusion, the surfaces of the TPU/graphene-based

composites change, see **Figure 3g-j**. This can only be attributed to the presence of graphene-based flakes close to the outermost polymer skin (thickness ~15 μm). Therefore, the incorporated graphene flakes are hardly visible in the SEM images in **Figure 3g-j**. After removal of the TPU skin, the graphene fillers become visible (see **Figure 3l-o**) and show similar dispersion, as seen in the cross-sectional images (**Figure 3b-e**).

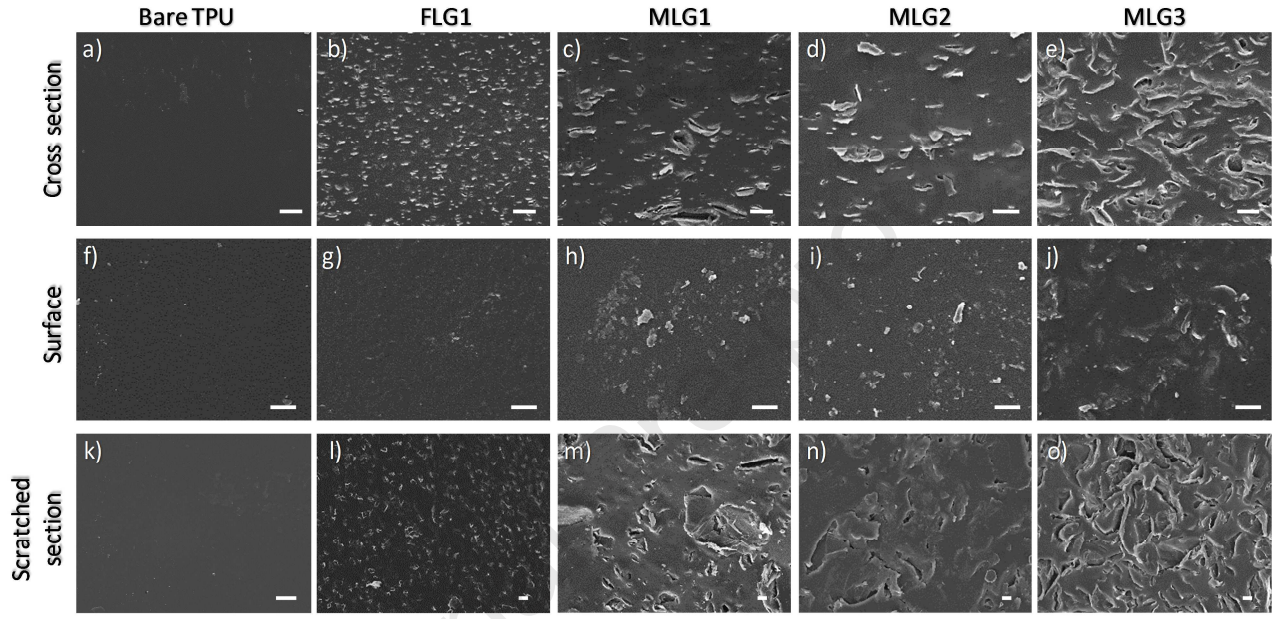

Figure 3. Cross-sectional, surface (with TPU skin) and scratched surface (without TPU skin) SEM images of bare TPU and TPU composites filled with FLG1, MLG1, MLG2, and MLG3 fillers at 4 wt.% concentration. The scale bars represent 10 μm.

3.2 Spectroscopy

Raman spectra of the neat TPU and TPU/graphene-based composites at 4 wt.% of filler content are shown in **Figure 4**. The neat TPU displays characteristic peaks at 1300 cm^{-1} associated with urethane linkage (amide III), 1445 cm^{-1} for symmetric stretching of N=C=O, and two broad peaks at 2855 cm^{-1} and 2927 cm^{-1} assigned to benzene ring vibrations, respectively[16,56]. Upon the addition of graphene-based fillers into the TPU matrices, new peaks appear in the spectra. The Raman spectrum of graphene-based materials mainly consist of the D (at ~1350 cm^{-1}), G (at ~1580 cm^{-1}), and 2D band (at ~2720 cm^{-1}) (see more details in **Supporting information, section SI-1**)[57–60]. In **Figure 4a**, all the graphite peaks are present for the four samples, the D band is barely

visible (found at ~1345 cm^{-1}) and has been increased ten folds. Besides to the TPU and graphene-related fingerprints, Raman spectroscopy is used to estimate the dispersion of the few-layer (FLG1) and multilayer graphene (MLG1, MLG2, and MLG3) fillers inside the TPU matrix[61,62]. For this, Raman mappings are performed on 100 µm × 100 µm scan areas and the intensity ratios of the 2D band (I_{2D}) at 2720 cm^{-1} from graphene and benzene ring (I_{TPU}) at 2855 cm^{-1} or 2927 cm^{-1} from TPU were used to visualize the graphene distribution into the polymer matrix. **Figure 4b** shows the intensity ratio (I_{2D}/I_{TPU}) maps obtained consisting in regions with $I_{2D}/I_{TPU} > 0.75$ red-colored and $I_{2D}/I_{TPU} < 0.35$ blue/violet-colored.

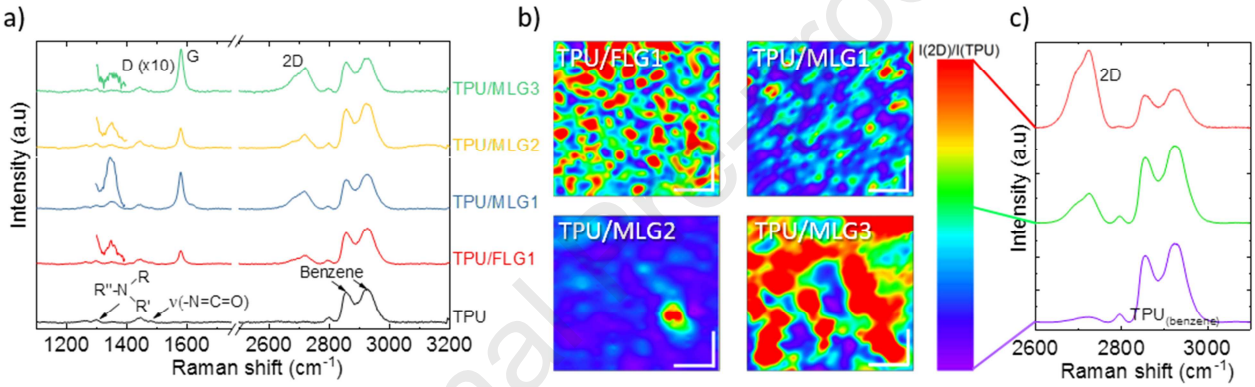

Figure 4. a) Raman spectra of the neat TPU and TPU loaded with FLG1, MLG1, MLG2, and MLG3 at 4 wt.%. Identifications of TPU vibrational modes and, G and 2D bands in graphene structure have been included. The spectra are normalized to the benzene bands of TPU. The inset shows the D band ten times amplified. b) Filler distribution (red-green) in the TPU polymer (blue-purple) obtained by Raman mapping on respective samples at 4 wt.% fillers concentration. All scale bars represent 25 µm. c) Raman spectra of the representative colors in the Raman maps.

In specific, the blue or violet colors in the maps are considered as an absence of the graphene flakes (FLG or MLG) on the surface, and green or red colors are related to a surface enriched with them. Raman spectra corresponding to each color in the distribution map are shown in **Figure 4c**. Here it is important to note that Raman mappings were performed on scratched surfaces (without TPU skin) to analyze the bulk dispersion. As seen in **Figure 4b**, the TPU/FLG1 sample (at 4 wt.%) demonstrates the homogeneous distribution of the graphene-based flakes on its surface. However,

the presence of red-green zones with blue regions all around them relates to the small flakes of the FLG1 powder (see **Table 1**). The samples TPU/MLG1 and TPU/MLG2, with 4 wt.% of MLG fillers, show higher proportions of the blue-violet colors, indicating graphene-free zones in the bulk composites, compared to the other samples. In contrast, the Raman map of the TPU/MLG3 sample demonstrates a higher filler population within the TPU matrix at equal concentration. The presence of polymer (blue-violet zones) is also visible. However, the overall surface is dominated by large graphene regions (red-green zones). The MLG3 sample, due to the large flake size and lateral size distribution ($D_L \approx$ 0.1-25.0 μm) cover the polymer film through flake-to-flake overlying. Qualitatively, ~75% surface is covered with MLG3 as quantified by the Raman map of the TPU/MLG3 sample. Whereas, the other samples TPU/FLG1, TPU/MLG1, and TPU/MLG2 show approximately ~68%, ~25%, and ~10% Raman signatures related to graphene modes, respectively. SEM images of the corresponding surfaces (see **Figure 3i-o**) also demonstrate similar findings and thus, validating the Raman mapping results. X-ray photoelectron spectroscopy (XPS) analysis of the graphene-based powders shows that the MLG3 sample has a higher amount of oxygenated (carbonyl, carboxyl, and carboxylic acid groups) species (~16.6%) and the oxygenated families are systematically reduced MLG3>MLG2>MLG1>FLG1 (~6.0%) (see details in **supporting information, Figure S4 and Table S1**).

3.3 Mechanical strength

Thermoplastic polyurethane is a versatile polymer with exceptional physical properties. For example, the measurements of pure TPU show elastic modulus, tensile strength, and maximum elongation at break of 5.6 MPa, 23.5 MPa, and 560%, respectively, as derived from the stress-strain curve in **Figure 5**. These values are consistent with previous studies[17,30]. The stress-strain properties of the TPU/graphene-based composites are also shown in **Figure 5**. For brevity, only two sets of the composites are given, namely TPU/FLG1 and TPU/MLG3, with different concentrations of the fillers, which are the ones with best fillers dispersion according to SEM imaging and Raman mapping. As shown in **Figure 5a**, when FLG1 is used at 1 wt.%, the TPU/FLG1 nanocomposite

demonstrates 34% and 162% improvements in tensile strength and Young modulus, respectively. The ultimate tensile strength increased from 23.5 MPa (for neat TPU) to ~30.9 MPa, while the Young modulus reached 14.7 MPa, starting from a value of 5.6 MPa. At this concentration, the maximum elongation at break of the TPU/FLG1 composite does not show any reduction, as seen in **Figure 5a**. However, at higher concentrations of FLG1 fillers, *i.e.*, 4 wt.% and 5 wt.%, the maximum elongation at break is reduced from 560% to 509% and 484%, respectively, while the Young modulus of these samples remain in a similar range (15.0-19.0 MPa), as shown in **Table 2**.

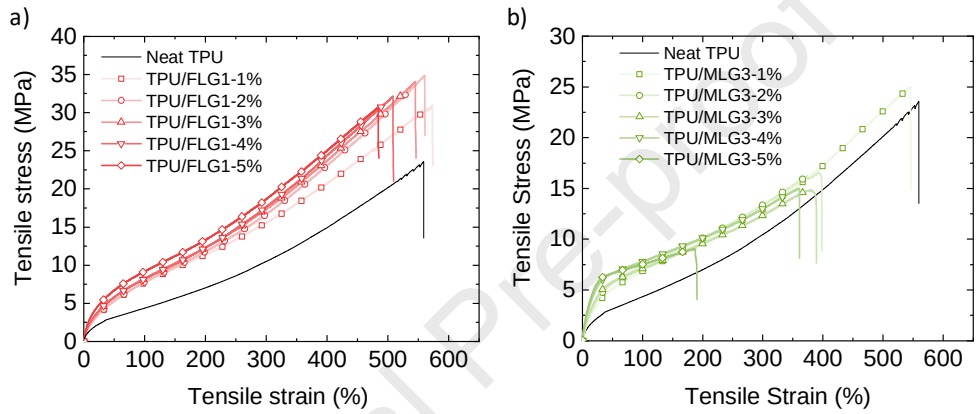

Figure 5. Stress-strain properties of the a) TPU/FLG1 and b) TPU/MLG3 composites at different filler contents. Neat TPU also has been included for comparison purposes.

Inversely, when TPU polymer is filled with MLG3 at different concentrations, the Young modulus of the as-prepared composites is increased significantly compared to the bare polymer. For example, at 1, 2, 3, and 4 wt.% of the MLG3 samples, the Young modulus is increased from 5.6 MPa (for pristine TPU) to 10.5, 17.9, 20.7, and 30.4 MPa, respectively (see **Table 2**). As indicated by the XPS analysis, the oxygenated moieties are present in large quantities in the MLG3 (~16.6%) and interact with the amine (N-H) groups of polymeric matrix (TPU) through H-bonding (see **supporting information section SI-4, Figure S5**), resulting in a significant improvement in the Young modulus of the respective composites[63,64]. However, contrary to the TPU/FLG1 composites, the TPU/MLG3 ones show a decrease in ultimate tensile strength and maximum elongation at break. For example, the ultimate tensile strength and maximum elongation at break are reduced from 23.5 MPa and 560% (for neat TPU) to 14.9 MPa and 360% respectively, for 4 wt.%

of MLG3, as summarised in **Table-2**. This corresponds to ~35% reduction in the respective mechanical properties. Moreover, the stress at a given strain in the TPU/MLG3 composites is always lower than that of the TPU/FLG1 composites (see **Figure 5**). This can be attributed to the multilayer graphene structure (> 8 layers in MLG3, see **Table 1**) and reduced stress transfer between the graphene layers[41,65]. It is also well accepted in literature that at fillers concentration > 1 wt.%, the Young modulus of the material increases, whereas, maximum elongation at break and, sometimes, ultimate tensile strength decays[6,29,41]. Further loading of the MLG3 graphene in the TPU polymer displayed a higher loss in mechanical strength and elongation values. For instance, the ultimate tensile strength is reduced to 9.0 MPa at 5 wt.% concentration of MGL3. For the same TPU/MLG3 nanocomposite, the maximum elongation at break is reduced to 186%. This significant decrease in the mechanical strength and maximum elongation at break of the TPU/MGL3 composites is associated with the large platelet size as well as the high filler contents (due to low bulk density) at this concentration[6,66,67]. Although the TPU/graphene-based composites (filled with FLG1 and MLG3) show substantial improvement in Young's modulus, the ultimate tensile strength and maximum elongation at break of the TPU/MLG3 composites show degradation as compared to the TPU/FLG1 composites. These composites (TPU/FLG1 and TPU/MLG3) can be used for packaging applications (food and electronics) in the form of multilayer structures[20].

Table 2. Summary of mechanical properties of the TPU/FLG1 and TPU/MLG3 composites.

Graphene-based flakes concentration	**Young Modulus (St. dev. ± 1.0 MPa)**		**Tensile strength (St. dev. ± 1.0 MPa)**		**Maximum elongation at break (St. dev. ± 10%)**	
(w/w) %	FLG1 (MPa)	MLG3 (MPa)	FLG1 (MPa)	MLG3 (MPa)	FLG1 %	MLG3 %
0 (Neat TPU)	5.6	5.6	23.5	23.5	560	560
1	14.7	10.5	30.9	24.9	573	546

2	14.6	17.9	34.8	16.5	561	393
3	16.0	20.7	34.0	14.8	546	379
4	15.9	30.4	32.1	14.9	509	360
5	18.7	46.0	30.7	9.0	484	186

3.4 Gas barrier properties

Similar to other semi-crystalline polymers, the gas permeability of the neat TPUs depends on solubility and diffusion coefficients of gas in the TPU film[51,68]. The chemical/physical composition of the TPUs (*e.g.*, hard/soft segments ratio, degree of cross-linking, etc.) plays an essential role in gas transportation[20]. When the TPU film is filled with impermeable nanofillers such as graphene-based flakes[69], gas solubility and diffusion coefficients of the TPU films are primarily influenced by the geometry and concentration of the nanofillers[34,35]. Therefore, in this study, four different graphene-based powders have been used to investigate the effect of lateral size (L), flake size distribution (D_L), and graphene-based flakes concentration on O_2 gas permeability of the TPU composites. **Figure 6a** shows O_2 gas permeability of the corresponding TPU/graphene-based composites as a function of the concentration of the filler. The neat TPU film shows a gas permeability of 144,846.44 mL.micron/m^2.day.atm (corresponding to 2.20 Barrer). All the TPU composites having different fillers demonstrate improved gas barrier properties compared to the neat TPU. For example, the TPU composites loaded with FLG1 display 20% and 39% reduction in O_2 gas permeability at concentrations of 1 wt.% and 4 wt.%, respectively. Similarly, when MLG1 is used, the prepared nanocomposite with 1 wt.% loading exhibits more than 50% reduction in the gas permeability, as shown in **Figure 6a**. However, further increase (up to 5 wt.%) of the MLG1 content did not produce any substantial improvement in the gas barrier properties.

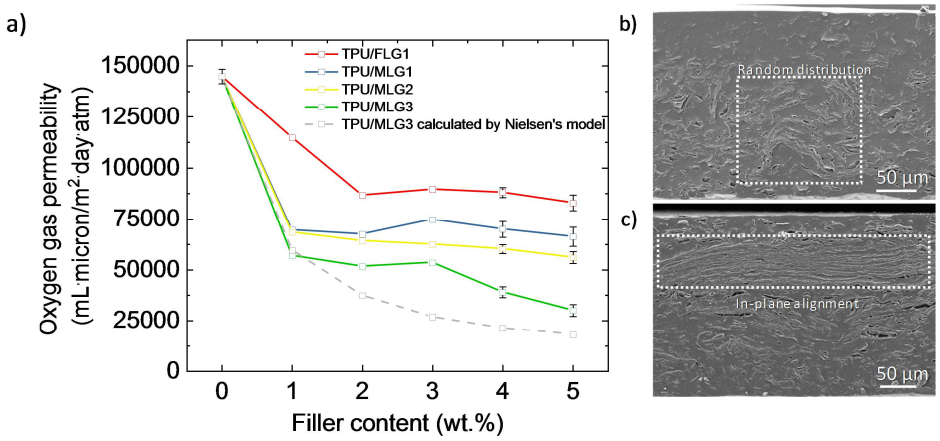

Figure 6. a) O_2 gas permeability of the TPU polymer filled with graphene-based flakes of different morphologies (FLG1, MLG1, MLG2, and MLG3). The dotted line represents the gas permeability of the TPU/MLG3 composites calculated with modified Nielsen's model [34,70]. SEM images of sample TPU/MLG3 b) before and c) after hot pressing. Hot pressing conditions are 3.0 metric tons pressing force, 150 °C temperature, and 30 minutes pressing time.

Gas barrier properties of the TPU/graphene-based composites prepared with the other MLG, namely MLG2 and MLG3, are also shown in **Figure 6a**. The TPU composites loaded with MLG2 show similar reduction in the gas permeability as the MLG1. It is noteworthy that, although there is a variation in the morphology of the flakes in FLG1, MLG1 and MLG2, the bulk densities and lateral size distributions are almost in the same range (*i.e.*, 0.04-0.06 g cm^{-3}, $D_L \approx$ 0.1-14.5 µm, see **Table 1**). In contrast, when TPU is loaded with MLG3 having $D_L \approx$ 0.1-25.0 µm and bulk density 0.012 g cm^{-3}, the O_2 gas permeability is reduced from 144,846.44 mL.micron/m^2.day.atm (for neat TPU) to 38,999.66 mL.micron/m^2.day.atm (or 0.59 Barrer) at 4 wt.% concentration, corresponding to 73% reduction. The MLG3 flakes have a broader size distribution with larger flakes (*i.e.*, 25.0 µm) compared to other fillers (≤ 14.5 µm). Therefore, it can be established that the substantial increase in the O_2 gas barrier properties of the TPU/MLG3 composites is attributed to several factors, *i.e.*, good dispersion, low bulk density, and broad size distribution of the fillers[52,71]. Further reduction in the gas permeability was also noticed at 5 wt.% of the MLG3 powder. However, at this concentration (*i.e.*, 5 wt.%) the tensile strength and maximum elongation at break

of the TPU/MLG3 composite are reduced by ~ 61% and ~ 66%, respectively, compared to the neat TPU as seen in **section 3.3**.

To achieve high barrier properties without a substantial decrease (> 35%) in the mechanical properties, the as-prepared TPU/MLG3 nanocomposite at 4 wt.% filler content was hot-pressed instead. The TPU/MLG3 composite was hot-pressed at 150 °C under 3.0 metric tons pressing force for 30 min. The hot-pressed TPU/MLG3 nanocomposite exhibited 8% further improvement in the gas barrier properties, leading to 81% total reduction in the O_2 gas permeability (corresponding to 27,520.82 mL.micron/m^2.day.atm or 0.42 Barrer). Likewise, the TPU composites filled with the other few-layer (FLG1) and multilayer graphene (MLG1 and MLG2) flakes also demonstrated 8-10% enhancement in gas barrier properties after hot pressing (see **supporting information, Figure S6**). The cross-sectional SEM images of the TPU/MLG3 nanocomposite (at 4 wt.%) before and after hot pressing are shown in **Figure 6b-c**. It is clear from the SEM images that the graphene-based flakes are randomly distributed in the as-prepared TPU/MLG3 nanocomposite, whereas, the hot-pressed sample demonstrates an *in*-plane alignment of the flakes. Consequently, the hot-pressed composites, TPU/FLG1 and TPU/MLG3, also exhibited 8% and 30% improvement in tensile strength as compared to the as-prepared samples, respectively. However, the Young modulus and maximum elongation improved only slightly (see **supporting information, Figure S7**).

For the theoretical estimation of the permeability profile of the TPU/graphene-based composites, a modified Nielsen's model was also used [34,70]. According to the modified Nielsen's equation, relative permeability (P/P_0) of a polymer film filled with platelet fillers can be defined as,

$$P/P_0 = \frac{1-\Phi_F}{1+\frac{\alpha}{3N}(S'+\frac{1}{2})\Phi_m} \qquad \text{(I)}$$

In which, P is the permeability of the filled polymer, P_0 is the permeability of the pristine polymer, α is the aspect ratio of the fillers (L/W), Φ_F is the volume fraction of the fillers, φ_m is the volume fraction of the matrix, N is the average number of graphene layers in a flake, and S' is the orientation of the fillers inside the polymer matrix (where $S' = 0$ for randomly oriented fillers and S'

= 1 for highly in-plane oriented fillers). The detailed information on the modified Nielsen's model and calculated permeability profiles of all TPU/graphene-based composites filled with FLG and MLG fillers are presented in the **supporting information section SI-7** and **Figure S8.** Herein, the calculated permeability profile of only TPU/MLG3 at different filler contents is plotted in **Figure 6a**. The theoretical results of the gas barrier properties of the TPU/MLG3 composites calculated from **equation (I)** reside close to the actual experimental results, as shown in **Figure 6a**. To estimate their statistical correlation, a two-sample t-test was also used to calculate the p-value[40,72]. The two data sets (theoretical and experimental) are considered to be significantly different when p-value < 0.05 (see further details in **supporting information, section SI-8**). Herein, the calculated p-value ~ 0.67 suggests the two permeability profiles (experimental and calculated) have a strong correlation and are not significantly different from each other. Therefore, low-quality MLG nanoplatelets with broad size distribution (for example, MLG3) can be regarded as ideal fillers to improve the gas barrier properties in the industrial packaging materials. Consequently, the TPU/MLG3 nanocomposite at 4 wt.% with Young modulus, tensile strength, and maximum elongation at break of ~30 MPa, ~15 MPa, and 358%, respectively, together with 81% reduction in oxygen gas permeability is suitable for multilayer packaging materials.

3.5 Thermogravimetric analysis

Thermal degradation of the urethane polymers occurs in two stages, corresponding to dissociation of the urethane linkage and then degradation of the polyol segments[73,74]. Initially, in the 200 – 250 °C temperature range, the self-coupling of isocyanate groups to form dimers and trimers has also been observed[29,75]. Afterward, at a higher temperature, *i.e.*, 300-375 °C, the first primary degradation process starts. This corresponds to cleavage of the urethane bonds to form isocyanates, polyols, and other nitrogen-containing products such as acetonitrile and acrylonitrile to name a few[75]. Whereas the second stage degradation of the polyol segments starts in the 380-410 °C temperature range, as shown in **Figure 7a**. After the inclusion of graphene-based fillers at 4 wt.%, the thermal stability of the TPU polymer appears to be improved at both degradation stages. For

example, the onset temperature $T_{10\%}$ (temperature for 10% weight loss) of the composites is ~ 20 °C higher than that of the neat TPU in the first degradation step. Meanwhile, the onset temperature $T_{80\%}$ for the second step of degradation for the composites is shifted towards higher temperatures by 10 to 15 °C, depending on the type of graphene-based flakes. Additionally, the rate of weight loss (weight derivative) is also slow at the second stage of degradation, as shown in **Figure 7a**.

The TPU nanocomposites loaded with 4 wt. % FLG1 are the only ones that display reduced thermal stability at this concentration with respect to neat TPU. Nevertheless, at higher FLG1 graphene loading of 5 wt. % the nanocomposites show comparable thermal stability to the neat TPU (see **supporting information, Figure S9**). In the case of MLG fillers, the overall thermal stability of all the nanocomposites is improved with respect to neat TPU. The impermeable graphene fillers obstruct the emission of the gaseous molecules produced during the pyrolysis of the TPU chains and result in the reduced degradation rate[76]. The residual percentage in **Figure 7a** also confirmed the nominal loading of the flakes (*i.e.*, 4 wt.%) in the TPU/graphene-based composites.

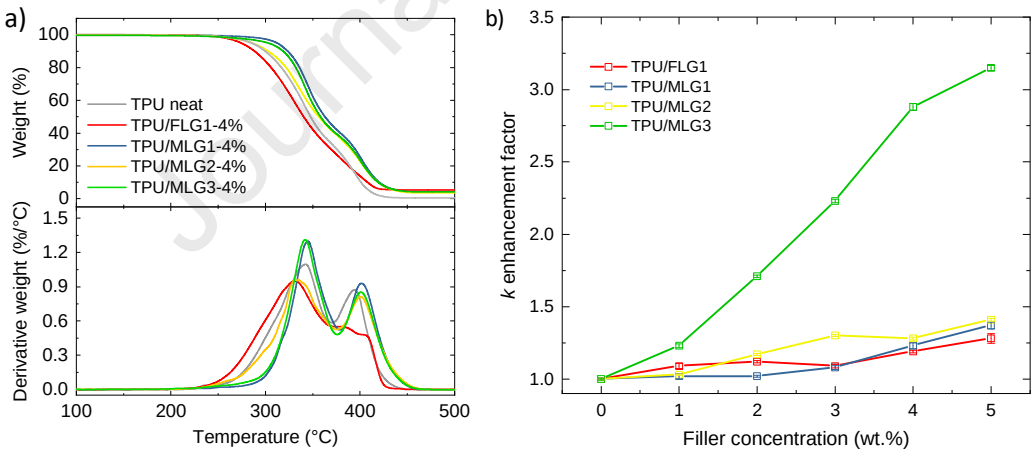

Figure 7. a) Thermogravimetric analysis of neat TPU and TPU with different graphene-based fillers at 4 wt.% loading. b) Enhancement in thermal conductivity (k) of the TPU/graphene-based composites.

3.6 Thermal conductivity

The enhancement in thermal conductivity (or relative thermal conductivity k/k_o) of the TPU/graphene composites is plotted against filler content in **Figure 7b**. To achieve this, coin-shaped samples (thickness ≈ 3 mm and diameter ≈ 20 mm) were prepared. After the flakes

inclusion, the thermal conductivity of the neat TPU is improved from $k_o \approx 0.26 \pm 0.01$ W m^{-1}K (for unfilled samples) to 0.31 ± 0.01, 0.32 ± 0.01, and 0.33 ± 0.02 W m^{-1}K at a concentration of 4 wt.% for FLG1, MLG1, and MLG2 corresponding to an increase of 19% ($k/k_o \approx 1.19$), 23% ($k/k_o \approx 1.23$), and 27% ($k/k_o \approx 1.27$), respectively. On the other contrary, the composite incorporating MLG3 demonstrates a significant increase in thermal conductivity reaching 0.74 ± 0.04 and 0.81 ± 0.01 W m^{-1}K at 4 wt.% and 5 wt.% corresponding to an improvement of 184% ($k/k_o \approx 2.84$) and 211% ($k/k_o \approx 3.11$), respectively, as shown in **Figure 7b**. The lower thermal conductivities of the TPU/graphene-based composites filled with FLG1, MLG1, and MLG2 fillers compared to the MLG3 one could be due to the small size of the graphene flakes and their arrangement in the composites (See SEM images in **Figure 3** and Raman maps in **Figure 4b**), lacking in connectivity of the flakes[77]. This causes poor thermal transportation as well as gas barrier properties, as seen in the previous **section 3.4**.

The exploitation of MLG3, with large lateral size and broad size distribution (D_L ~ 0.1-25.0 μm) of the flakes, allows the optimization of the packing density throughout the TPU matrix and enhances the thermal conductivity of the final nanocomposite in addition to its gas barrier properties[6,43]. The mechanical properties of the sample TPU/MLG3 at 4 wt.% (elongation at break 360% and ultimate tensile strength 15 MPa).

4. Conclusion

In this work, the effect of the morphology (lateral size and size distribution) of graphene-based fillers is investigated on the gas barrier, mechanical, and thermal properties of the TPU composites. In this regard, few-layer graphene and three multilayer graphene powders are used. The TPU/graphene-based composites are prepared through the solution blending technique. The composite prepared with multilayer graphene (MLG3) having lateral size distribution between 0.1-25.0 μm demonstrated more than four times enhancement in the Young modulus and approximately three times improvement in thermal conductivity at 4 wt.% of the filler content, compared to the neat polymer. Moreover, the same composite exhibited ~81% reduction in O_2 gas permeability after

hot-pressing. In contrast, when few-layer graphene or multilayer graphene powders with narrow size distributions are incorporated into the TPU matrix, the gas barrier and thermal properties are inferior compared to the ones obtained with the larger flakes. The prepared multilayer graphene-based composites with enhanced O_2 gas barrier, mechanical, and thermal properties have been envisioned for packaging applications.

Conflicts of interest: There are no conflicts of interest to declare.

Acknowledgement: "This research work has received funding from the European Union's Horizon 2020 research and innovation program under grant agreement No. 785219 – Graphene Flagship Core2". The authors also thank Avanzare (Spain) for donating free samples.

Appendix A. (Supplementary data): A supporting information file is provided with this manuscript.

References

[1] S.S. Pendhari, T. Kant, Y.M. Desai, Application of polymer composites in civil construction: A general review, Compos. Struct. 84 (2008) 114–124. doi:10.1016/J.COMPSTRUCT.2007.06.007.

[2] P.D. Mangalgiri, Composite materials for aerospace applications, Bull. Mater. Sci. 22 (1999) 657–664. doi:10.1007/BF02749982.

[3] J.M. Garcés, D.J. Moll, J. Bicerano, R. Fibiger, D.G. McLeod, Polymeric nanocomposites for automotive applications, Adv. Mater. 12 (2000) 1835–1839. doi:10.1002/1521-4095(200012)12:23<1835::AID-ADMA1835>3.0.CO;2-T.

[4] Y. Sun, G. Shi, Graphene/polymer composites for energy applications, J. Polym. Sci. Part B Polym. Phys. 51 (2013) 231–253. doi:10.1002/polb.23226.

[5] J. Lange, Y. Wyser, Recent innovations in barrier technologies for plastic packaging?a review, Packag. Technol. Sci. 16 (2003) 149–158. doi:10.1002/pts.621.

[6] J.R. Potts, D.R. Dreyer, C.W. Bielawski, R.S. Ruoff, Graphene-based polymer nanocomposites, Polymer (Guildf). 52 (2011) 5–25. doi:10.1016/j.polymer.2010.11.042.

[7] L. Wang, S. Kanesalingam, R. Nayak, R. Padhye, Recent Trends in Ballistic Protection, Text. Light Ind. Sci. Technol. 3 (2014) 37. doi:10.14355/tlist.2014.03.007.

[8] R. Siddique, J. Khatib, I. Kaur, Use of recycled plastic in concrete: A review, Waste Manag. 28 (2008) 1835–1852. doi:10.1016/j.wasman.2007.09.011.

[9] B. Geueke, K. Groh, J. Muncke, Food packaging in the circular economy: Overview of chemical safety aspects for commonly used materials, J. Clean. Prod. 193 (2018) 491–505. doi:10.1016/j.jclepro.2018.05.005.

[10] PlasticsEurope, Annual Review 2017-2018, Assoc. Plast. Manuf. 15 (2018) 44. https://www.plasticseurope.org/download_file/force/1830/181.

[11] J. Hammer, M.H.S. Kraak, J.R. Parsons, Plastics in the marine environment: The dark side of a modern gift, Rev. Environ. Contam. Toxicol. 233 (2015) 1–44. doi:10.1007/978-3-319-10479-9.

[12] J. Lagaron, M. Sanchez-Garcia, E. Gimenez, Thermoplastic nanobiocomposites for rigid and flexible food packaging applications, in: Environ. Compat. Food Packag., Woodhead Publishing, 2008: pp. 63–89. doi:10.1533/9781845694784.1.63.

[13] G.T. Howard, Biodegradation of polyurethane: A review, Int. Biodeterior. Biodegrad. 49 (2002) 245–252. doi:10.1016/S0964-8305(02)00051-3.

[14] J.P. Santerre, K. Woodhouse, G. Laroche, R.S. Labow, Understanding the biodegradation of polyurethanes: From classical implants to tissue engineering materials, Biomaterials. 26 (2005) 7457–7470. doi:10.1016/j.biomaterials.2005.05.079.

[15] N. Mahajan, P. Gupta, New insights into the microbial degradation of polyurethanes, RSC Adv. 5 (2015) 41839–41854. doi:10.1039/c5ra04589d.

[16] H.-Y. Mi, X. Jing, M.R. Salick, T.M. Cordie, L.-S. Turng, Carbon nanotube (CNT) and nanofibrillated cellulose (NFC) reinforcement effect on thermoplastic polyurethane (TPU) scaffolds fabricated via phase separation using dimethyl sulfoxide (DMSO) as solvent, J. Mech. Behav. Biomed. Mater. 62 (2016) 417–427. doi:10.1016/j.jmbbm.2016.05.026.

[17] M. Bera, P.K. Maji, Effect of structural disparity of graphene-based materials on thermo-mechanical and surface properties of thermoplastic polyurethane nanocomposites, Polymer (Guildf). 119 (2017) 118–133. doi:10.1016/j.polymer.2017.05.019.

[18] V.K. Aswal, P. Maiti, K.K. Jana, S. Pandey, D. Rana, Effect of nanoparticle on the mechanical and gas barrier properties of thermoplastic polyurethane, Appl. Clay Sci. 146 (2017) 468–474. doi:10.1016/j.clay.2017.07.001.

[19] P. Bandyopadhyay, T.T. Nguyen, X. Li, N.H. Kim, J.H. Lee, Enhanced hydrogen gas barrier performance of diaminoalkane functionalized stitched graphene oxide/polyurethane Composites, Compos. Part B. 117 (2017) 101–110.

[20] M. Joshi, B. Adak, B.S. Butola, Polyurethane nanocomposite based gas barrier films, membranes and coatings: A review on synthesis, characterization and potential applications, Prog. Mater. Sci. 97 (2018) 230–282. doi:10.1016/j.pmatsci.2018.05.001.

[21] R.A. Zoppi, S. Das Neves, S.P. Nunes, Hybrid films of poly(ethylene oxide-b-amide-6) containing sol-gel-silicon or titanium oxide as inorganic fillers: Effect of morphology and mechanical properties on gas permeability, Polymer (Guildf). 41 (2000) 5461–5470. doi:10.1016/S0032-3861(99)00751-X.

[22] V. Vladimirov, C. Betchev, A. Vassiliou, G. Papageorgiou, D. Bikiaris, Dynamic mechanical and morphological studies of isotactic polypropylene/fumed silica nanocomposites with enhanced gas barrier properties, Compos. Sci. Technol. 66 (2006) 2935–2944. doi:10.1016/j.compscitech.2006.02.010.

[23] A. Ali, K. Yusoh, S.F. Hasany, Synthesis and physicochemical behaviour of polyurethane-multiwalled carbon nanotubes nanocomposites based on renewable castor oil polyols, J. Nanomater. 2014 (2014). doi:10.1155/2014/564384.

[24] A.C. Ferrari, F. Bonaccorso, V. Fal'ko, K.S. Novoselov, S. Roche, P. Bøggild, *et al.*, Science and technology roadmap for graphene, related two-dimensional crystals, and hybrid systems, Nanoscale. 7 (2015) 4598–4810. doi:10.1039/c4nr01600a.

[25] G. Shamini, K. Yusoh, Gas permeability properties of thermoplastic polyurethane modified clay nanocomposites, Int. J. Chem. Eng. Appl. 5 (2014) 64–68. doi:10.7763/ijcea.2014.v5.352.

[26] M. Azeem, R. Jan, S. Farrukh, A. Hussain, Improving gas barrier properties with boron nitride nanosheets in polymer-composites, Results Phys. 12 (2019) 1535–1541. doi:10.1016/j.rinp.2019.01.057.

[27] D. Cai, K. Yusoh, M. Song, The mechanical properties and morphology of a graphite oxide nanoplatelet/polyurethane composite, Nanotechnology. 20 (2009). doi:10.1088/0957-4484/20/8/085712.

[28] H. Kim, Y. Miura, C.W. MacOsko, Graphene/polyurethane nanocomposites for improved gas barrier and electrical conductivity, Chem. Mater. 22 (2010) 3441–3450. doi:10.1021/cm100477v.

[29] J.N. Gavgani, H. Adelnia, M.M. Gudarzi, Intumescent flame retardant polyurethane/reduced graphene oxide composites with improved mechanical, thermal, and barrier properties, J. Mater. Sci. 49 (2014) 243–254. doi:10.1007/s10853-013-7698-6.

[30] P. Kaveh, M. Mortezaei, M. Barikani, G. Khanbabaei, Low-temperature flexible polyurethane/graphene oxide nanocomposites: Effect of polyols and graphene oxide on physicomechanical properties and gas permeability, Polym. - Plast. Technol. Eng. 53 (2014) 278–289. doi:10.1080/03602559.2013.844241.

[31] B. Min Yoo, J. Eun Shin, H. Dae Lee, H. Bum Park, Graphene and graphene oxide membranes for gas separation applications, Curr. Opin. Chem. Eng. 16 (2017) 39–47. doi:10.1016/j.coche.2017.04.004.

[32] M. Salzano de Luna, Y. Wang, T. Zhai, L. Verdolotti, G.G. Buonocore, M. Lavorgna, *et al.*, Nanocomposite polymeric materials with 3D graphene-based architectures: from design strategies to tailored properties and potential applications, Prog. Polym. Sci. 89 (2019) 213–249. doi:10.1016/j.progpolymsci.2018.11.002.

[33] G. Scherillo, M. Lavorgna, G.G. Buonocore, Y.H. Zhan, H.S. Xia, G. Mensitieri, *et al.*, Tailoring assembly of reduced graphene oxide nanosheets to control gas barrier properties of natural rubber nanocomposites, ACS Appl. Mater. Interfaces. 6 (2014) 2230–2234. doi:10.1021/am405768m.

[34] B.M. Yoo, H.J. Shin, H.W. Yoon, H.B. Park, Graphene and graphene oxide and their uses in barrier polymers, J. Appl. Polym. Sci. 131 (2014) 1–23. doi:10.1002/app.39628.

[35] Y. Cui, S.I. Kundalwal, S. Kumar, Gas barrier performance of graphene/polymer nanocomposites, Carbon N. Y. 98 (2016) 313–333.

[36] J.-H. Chang, Y.U. An, Nanocomposites of polyurethane with various organoclays: Thermomechanical properties, morphology, and gas permeability, J. Polym. Sci. Part B Polym. Phys. 40 (2002) 670–677. doi:10.1002/polb.10124.

[37] C. Xiang, P.J. Cox, A. Kukovecz, B. Genorio, D.P. Hashim, Z. Yan, *et al.*, Functionalized low defect graphene nanoribbons and polyurethane composite film for improved gas barrier and mechanical performances, ACS Nano. 7 (2013) 10380–10386. doi:10.1021/nn404843n.

[38] A. Kovtun, E. Treossi, N. Mirotta, A. Scidà, A. Liscio, M. Christian, *et al.*, Benchmarking of graphene-based materials: Real commercial products versus ideal graphene, 2D Mater. 6 (2019). doi:10.1088/2053-1583/aafc6e.

[39] A.P. Kauling, A.T. Seefeldt, D.P. Pisoni, R.C. Pradeep, R. Bentini, R.V.B. Oliveira, *et al.*, The worldwide graphene flake production, Adv. Mater. 30 (2018) 1803784–1803789. doi:10.1002/adma.201803784.

[40] M. Zahid, M.T. Masood, A. Athanassiou, I.S. Bayer, Sustainable thermal interface materials from recycled cotton textiles and graphene nanoplatelets, 113 (2018) 44103. doi:10.1063/1.5044719.

[41] K.S. Novoselov, L. Gong, I. a. Kinloch, R.J. Young, The mechanics of graphene nanocomposites: A review, Compos. Sci. Technol. 72 (2012) 1459–1476. doi:10.1016/j.compscitech.2012.05.005.

[42] J.G. Um, Y.S. Jun, A. Elkamel, A. Yu, Engineering investigation for the size effect of graphene oxide derived from graphene nanoplatelets in polyurethane composites, Can. J. Chem. Eng. (2019) 1–13. doi:10.1002/cjce.23696.

[43] J. Du, H.-M. Cheng, The fabrication, properties, and uses of graphene/polymer composites, Macromol. Chem. Phys. 213 (2012) 1060–1077. doi:10.1002/macp.

[44] P. Mukhopadhyay, R.K. Gupta, Trends and frontiers in graphene-based polymer nanocomposites, Plast. Eng. 67 (2018) 32–42. doi:10.1002/j.1941-9635.2011.tb00669.x.

[45] M. Terrones, O. Martín, M. González, J. Pozuelo, B. Serrano, J.C. Cabanelas, *et al.*, Interphases in graphene polymer-based nanocomposites: Achievements and challenges, Adv. Mater. 23 (2011) 5302–5310. doi:10.1002/adma.201102036.

[46] A.E. Del Rio Castillo, V. Pellegrini, A. Ansaldo, F. Ricciardella, H. Sun, L. Marasco, *et al.*, High-yield production of 2D crystals by wet-jet milling, Mater. Horizons. 5 (2018) 890–904. doi:10.1039/C8MH00487K.

[47] S. Bellani, E. Petroni, A.E. Del Rio Castillo, N. Curreli, B. Martín-García, R. Oropesa-Nuñez, *et al.*, Scalable Production of Graphene Inks via Wet-Jet Milling Exfoliation for Screen-Printed Micro-Supercapacitors, Adv. Funct. Mater. 29 (2019) 1807659. doi:10.1002/adfm.201807659.

[48] J. Hansson, T.M. J Nilsson, L. Ye, J. Liu, Novel nanostructured thermal interface materials: a review, Int. Mater. Rev. 0 (2016). doi:10.1080/09506608.2017.1301014.

[49] C. Wolf, H. Angellier-Coussy, N. Gontard, F. Doghieri, V. Guillard, How the shape of fillers affects the barrier properties of polymer/non-porous particles nanocomposites: A review, J. Memb. Sci. 556 (2018) 393–418. doi:10.1016/j.memsci.2018.03.085.

[50] N.K. Lape, E.E. Nuxoll, E.L. Cussler, Polydisperse flakes in barrier films, J. Memb. Sci. 236 (2004) 29–37. doi:10.1016/j.memsci.2003.12.026.

[51] O.C. Compton, S. Kim, C. Pierre, J.M. Torkelson, S.T. Nguyen, Crumpled graphene nanosheets as highly effective barrier property enhancers, Adv. Mater. 22 (2010) 4759–4763. doi:10.1002/adma.201000960.

[52] H.W. Kim, H.W. Yoon, S. Yoon, B.M. Yoo, B.K. Ahn, Y.H. Cho, *et al.*, Selective Gas Transport Through Few-Layered Graphene and Graphene Oxide Membranes, Science (80-.). 342 (2013) 91–95. doi:10.1126/science.1236098.

[53] G. Luo, X. Gu, J. Zhang, R. Zhang, Q. Shen, M. Li, L. Zhang, Microstructural, mechanical, and thermal-insulation properties of poly(methyl methacrylate)/silica aerogel bimodal cellular foams, J. Appl. Polym. Sci. 134 (2017) 1–7. doi:10.1002/app.44434.

[54] N. Mehra, Y. Li, X. Yang, J. Li, M.A. Kashfipour, J. Gu, *et al.*, Engineering molecular interaction in polymeric hybrids: Effect of thermal linker and polymer chain structure on thermal conduction, Compos. Part B Eng. 166 (2019) 509–515. doi:10.1016/j.compositesb.2019.02.029.

[55] B.M. Cromer, E.B. Coughlin, A.J. Lesser, Evaluation of a new processing method for improved nanocomposite dispersions, Nanocomposites. 1 (2015) 152–159. doi:10.1179/2055033215Y.0000000009.

[56] S. Parnell, K. Min, M. Cakmak, Kinetic studies of polyurethane polymerization with Raman spectroscopy, Polymer (Guildf). 44 (2003) 5137–5144. doi:10.1016/S0032-3861(03)00468-3.

[57] A.C. Ferrari, J.C. Meyer, V. Scardaci, C. Casiraghi, M. Lazzeri, F. Mauri, *et al.*, Raman spectrum of graphene and graphene layers, Phys. Rev. Lett. 97 (2006) 1–4. doi:10.1103/PhysRevLett.97.187401.

[58] A.C. Ferrari, J. Robertson, Resonant Raman spectroscopy of disordered, amorphous, and diamondlike carbon, Phys. Rev. B. 64 (2001) 075414. doi:10.1103/PhysRevB.64.075414.

[59] A.C. Ferrari, J. Robertson, Interpretation of Raman spectra of disordered and amorphous carbon, Phys. Rev. B. 61 (2000) 95–107.

[60] F. Bonaccorso, P.H. Tan, A.C. Ferrari, Multiwall nanotubes, multilayers, and hybrid nanostructures: New

frontiers for technology and Raman spectroscopy, ACS Nano. 7 (2013) 1838–1844. doi:10.1021/nn400758r.

[61] S.A. Shojaee, A. Zandiatashbar, N. Koratkar, D.A. Lucca, Raman spectroscopic imaging of graphene dispersion in polymer composites, Carbon N. Y. 62 (2013) 510–513. doi:10.1016/j.carbon.2013.05.068.

[62] M. Szybowicz, A.B. Nowicka, M. Sądej, E. Andrzejewska, M. Drozdowski, Morphology of polyacrylate/nanosilica composites as studied by micro-Raman spectroscopy, J. Mol. Struct. 1070 (2014) 131–136. doi:10.1016/j.molstruc.2014.04.062.

[63] H. Liu, Y. Li, K. Dai, G. Zheng, C. Liu, C. Shen, *et al.*, Electrically conductive thermoplastic elastomer nanocomposites at ultralow graphene loading levels for strain sensor applications, J. Mater. Chem. C. 4 (2015) 157–166. doi:10.1039/c5tc02751a.

[64] M. Strankowski, P. Korzeniewski, J. Strankowska, A.S. Anu, S. Thomas, Morphology, mechanical and thermal properties of thermoplastic polyurethane containing reduced graphene oxide and graphene nanoplatelets, Materials (Basel). 11 (2018). doi:10.3390/ma11010082.

[65] C. Lee, Q. Li, W. Kalb, X.Z. Liu, H. Berger, R.W. Carpick, *et al.*, Frictional characteristics of atomically thin sheets, Science (80-.). 328 (2010) 76–80. doi:10.1126/science.1184167.

[66] M. Bhattacharya, Polymer nanocomposites-A comparison between carbon nanotubes, graphene, and clay as nanofillers, Materials (Basel). 9 (2016) 1–35. doi:10.3390/ma9040262.

[67] U. Khan, P. May, A. O'Neill, J.N. Coleman, Development of stiff, strong, yet tough composites by the addition of solvent exfoliated graphene to polyurethane, Carbon N. Y. 48 (2010) 4035–4041. doi:10.1016/j.carbon.2010.07.008.

[68] J.G. Wijmans, R.W. Baker, The solution-diffusion model: a review, J. Memb. Sci. 107 (1995) 1–21. doi:10.1016/S0166-4115(08)60038-2.

[69] V. Berry, Impermeability of graphene and its applications, Carbon N. Y. 62 (2013) 1–10. doi:10.1016/j.carbon.2013.05.052.

[70] R.K. Bharadwaj, Modeling the barrier properties of polymer-layered silicate nanocomposites, Macromolecules. 34 (2001) 9189–9192. doi:10.1021/ma010780b.

[71] K.K. Sadasivuni, D. Ponnamma, S. Thomas, Y. Grohens, Evolution from graphite to graphene elastomer composites, Prog. Polym. Sci. 39 (2014) 749–780. doi:10.1016/J.PROGPOLYMSCI.2013.08.003.

[72] S.K. Misra, D. Mohn, T.J. Brunner, W.J. Stark, S.E. Philip, I. Roy, *et al.*, Comparison of nanoscale and microscale bioactive glass on the properties of P(3HB)/Bioglass®composites, Biomaterials. 29 (2008) 1750–1761. doi:10.1016/j.biomaterials.2007.12.040.

[73] S. Anandhan, H.S. Lee, Influence of organically modified clay mineral on domain structure and properties of segmented thermoplastic polyurethane elastomer, J. Elastomers Plast. 46 (2014) 217–232. doi:10.1177/0095244312465300.

[74] H. Liu, W. Huang, X. Yang, K. Dai, G. Zheng, C. Liu, *et al.*, Organic vapor sensing behaviors of conductive thermoplastic polyurethane-graphene nanocomposites, J. Mater. Chem. C. 4 (2016) 4459–4469. doi:10.1039/c6tc00987e.

[75] M. Herrera, G. Matuschek, A. Kettrup, Thermal degradation of thermoplastic polyurethane elastomers (TPU) based on MDI, Polym. Degrad. Stab. 78 (2002) 323–331. doi:10.1016/S0141-3910(02)00181-7.

[76] D.G. Papageorgiou, I.A. Kinloch, R.J. Young, Graphene/elastomer nanocomposites, Carbon N. Y. 95 (2015) 460–484. doi:10.1016/J.CARBON.2015.08.055.

[77] A. Li, C. Zhang, Y.F. Zhang, Thermal conductivity of graphene-polymer composites: Mechanisms, properties,

and applications, Polymers (Basel). 9 (2017). doi:10.3390/polym9090437.

Declaration of interests

☒ The authors declare that they have no known competing financial interests or personal relationships that could have appeared to influence the work reported in this paper.

☐The authors declare the following financial interests/personal relationships which may be considered as potential competing interests:

TOC